A Survey of Graph Cuts/Graph Search Based Medical Image Segmentation

Xinjian Chen, *Senior Member, IEEE*, and Lingjiao Pan

Abstract—**Medical image segmentation is a fundamental and challenging problem for analyzing medical images. Among different existing medical image segmentation methods, graph-based approaches are relatively new and show good features in clinical applications. In the graph-based method, pixels or regions in the original image are interpreted into nodes in a graph. By considering Markov random field to model the contexture information of the image, the medical image segmentation problem can be transformed into a graph-based energy minimization problem. This problem can be solved by the use of minimum *s-t* cut/ maximum flow algorithm. This review is devoted to cut-based medical segmentation methods, including graph cuts and graph search for region and surface segmentation. Different varieties of cut-based methods, including graph-cuts-based methods, model integrated graph cuts methods, graph-search-based methods, and graph search/graph cuts based methods, are systematically reviewed. Graph cuts and graph search with deep learning technique are also discussed.**

Index Terms—**Graph cuts (GCs), graph search (GS), medical image, segmentation.**

I. INTRODUCTION

MEDICAL image segmentation has received much research attention due to its valuable applications in clinical studies. In particular, medical image segmentation can be used for guiding computer-assisted diagnosis and treatment and quantitatively monitoring of disease progression [1]–[5]. Despite several decades of research work and many key advances, several challenges still remain in this area. These challenges can

be attributed to several factors. First, the anatomical structures of human organs are complex. They may consist of several different structures with different intensities, as seen for example in the kidnet, which consists of four major structures: renal cortex, renal column, renal medulla, and renal pelvis. Second, adjacent organs or organ structures may be connected and have very similar intensity. Third, boundaries between adjacent organs, such as the spleen and liver, may often be blurred. Finally, image artifacts and signal-degrading noises can confound segmentation techniques. Therefore, efficient, robust, and automatic segmentation of anatomy on radiological images is still very challenging.

There many current medical image segmentation methods: thresholding method [6]–[10], region growing method [11]–[14], edge detection method [15]–[17] are the most commonly used. Along with these traditional methods, there are various advanced approaches, including model-based methods, partial differential equations (PDE)-based methods, and graph-based methods. The representatives in model-based group are active shape models (ASM) [18]–[22] and active appearance models (AAM) [23]–[27]. The ASM/AAM methods use "landmarks" to represent shape and principal component analysis (PCA) to capture the major modes of variation in shape observed in the training datasets. In PDE-based methods, level sets are an important category of techniques [28]–[32]. They calculate the desirable segmentation result by evolving initial parametric curves in the continuous space according to the energy function until the energy function is minimized. Graph-based segmentation approaches play an important role in medical image segmentation. Typical graph-based segmentation algorithms include minimum spanning tree (MST)-based methods [33]–[36], shortest-paths-based methods [37]–[41], graph-cuts (GCs) approaches [42]–[53], among others. Among all the graph-based segmentation methods, GCs are relatively new and arguably the most powerful mechanisms [54]. A detail discussion and comparison of these segmentation methods can be found in [55]–[60].

Despite much effort devoted to the study of medical image segmentation methods, little work has been done to review the work in cut-based field. In this review, we mainly focus on cut-based medical segmentation methods, including GCs and graph search (GS) for region and surface segmentation separately. Compared to other documents that cover the theoretical aspects of image processing and analysis through the use of graphs in the representation and analysis of objects [137], [138], our paper has some novel points.

X. Chen is with the School of Electronic and Information Engineering, Soochow University, Suzhou 215000, China (e-mail: xjchen@suda.edu.cn).

L. Pan is with the School of Electronic and Information Engineering, Soochow University, Suzhou 215000, China, and also with the School of Electrical and Information Engineering, Jiangsu University of Technology, Jiangsu 212003, China (e-mail: 20154028001@stu.suda.edu.cn).

Digital Object Identifier 10.1109/RBME.2018.2798701

1) This paper systematically reviews cut-based methods, which are designed for specific biomedical imaging applications, especially GCs technique and GS technique for region and surface segmentation. Different varieties of cut-based methods (including GCs-based methods, model integrated GCs methods, GS-based methods, and GS /GCs-based methods) are systematically reviewed. We not only cover the basic theory of GCs and GS but also discuss the relationship and differences between GCs and GS.

2) This paper not only introduces optimal single-surface, single-object, multisurface, and multiobject image segmentation methods, but also adds the discussion of multimodality segmentation. We systematically review the research for dealing with the cosegmentation problem. How to fully utilize the characteristics of multimodality medical images is introduced and the different ways to construct the graph are discussed.

3) Many new algorithms and concepts that have been recently published are included in this paper. We cover work for biomedical imaging applications using GCs and GS method combine with the deep learning technique. How to combine the deep learning technique with GCs and GS method and how to embody the robustness of deep learning while retaining the advantage of the traditional graph-based methods can be studied from these reviewed works.

The rest of this review is organized as follows. In Section II, we review medical image segmentation approaches using GCs. In Section III, GCs-based hybrid methods are described. In Section IV, we present medical image segmentation approaches using GS. In Section V, how to synergistically combine the GS and GCs methods to solve more complex and challenging medical image segmentation problems are well discussed. In the final section, these graph-based medical image segmentation approaches are concluded, and some issues related to the future of the cut-based medical image segmentation are discussed.

II. GCS-BASED SEGMENTATION

A. Background

Graph-based segmentation approaches play an important role in medical image segmentation. A graph interprets pixels or regions in the original image into nodes in the graph. Then, the segmentation problem can be transformed into a labeling problem which requires assigning correct label to each node according to its properties. Markov random field (MRF) is successfully used in computer vision and machine learning to model contexture information of pixels. This contexture information provides a mechanism for obtaining image properties. Combined with the Bayesian maximum a posterior (MAP) estimation, the MAP–MRF framework [61] formulates the labeling problem as a graph-based minimization problem. GCs provide a flexible optimization tool to solve the minimization problem with computational efficiency.
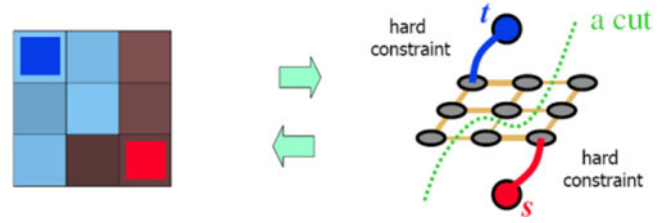

Fig. 1. Illustration of graph construction for simple 2-D image. (This figure is from Boykov's ECCV 2006 tutorial. http://www.csd. uwo.ca/faculty/yuri/Presentations/ECCV06_tutorial_partI_yuri.pdf.)

A graph $G = (V, E)$ is a general structure consisting of a set of nodes (or vertexes) V corresponding to pixels/voxels of original image and a set of arcs (or edges) E connecting neighboring nodes. Every arc has a nonnegative weight or cost representing a kind of measurement of quantity based on the property of two neighboring vertexes connected by edge. A cost of a directed edge may differ from the cost of the reverse edge. A simple two-dimensional (2-D) image example is shown in Fig. 1. In addition to nodes set V, there are two special terminal nodes, called source s and sink t which represent "object" and "background" separately in biobject segmentation. The arcs set E in a graph G includes two kinds of arcs. The first type namely n-links where "n" stands for "neighbor," which connects neighboring pixels. The second type t-links where "t" stands for "terminal," which connects pixels and terminals.

An s/t cut in a graph G is a partitioning of V into two disjoint subsets S and T such that all object voxels are connected to an object terminal node s and all background voxels are connected to a background terminal node t. The goal is to find the best cut that could give an optimal result according to the segmentation requirement. A cut with the minimal cost is the minimal cut and is also the best cut. The best cut can be obtained by minimizing the following energy function which consider both regional and boundary properties

$$E(L) = \sum_{p \in P} R_p(L_p) + \sum_{(p,q) \in N} B_{pq}(L_p, L_q). \quad (1)$$

In the above equation, L_p is the label of pixel p in an image P. The first term is a regional term and $R_p(L_p)$ is the penalty to assign label L_p to pixel p. If labels are correctly assigned to all the pixels, the region energy function should reach the minimal value. The second term is a boundary term $B_{pq}(L_p, L_q)$, which can be interpreted as a penalty for discontinuity between p and q. Generally speaking, $B_{pq}(L_p, L_q)$ is large when p and q are similar. And $B_{pq}(L_p, L_q)$ is close to zero when p and q are totally different. In another word, if p and q are similar, then the probability that they belong to the same object is high. Otherwise, p and q may belong to different objects. Therefore, boundary energy is small if neighboring pixels p and q are different. As mentioned before, there are two kinds of edges: n-links and t-links. The n-links connect neighboring pixels. Their cost can represent the boundary characteristic and can be derived from the boundary term. The t-links connect pixels and terminals. Their cost represents the regional characteristic and can be obtained from the regional term.

Several algorithms can be used to solve this combinatorial optimization problem [62]–[65]. Most of them can be categorized in one of the following two groups: push relabel methods [66] and augmenting path methods [62]. Boykov *et al.*'s augmenting-path-based algorithm [54] shows better performance compared to other algorithms. Before *s/t* GCs approach, computing global optima was only possible for some 2-D object segmentation methods [67]. Up to now, *s/t* GCs technique and its variants have been widely used to solve many 3-D segmentation problems in medical image areas.

B. Single-Object Segmentation

In medical image, specific tissues or organs of interest usually need to be extracted for medical diagnosis. In the single-object segmentation case, it is a binary labeling problem. This problem can be solved efficiently with GCs in polynomial time when B_{pq} is a submodular function, i.e., $B_{pq}(0, 0) + B_{pq}(1, 1) \leq B_{pq}(0, 1) + B_{pq}(1, 0)$ [68]. The early work was done by Boykov *et al.* where single object or multiobjects were segmented in both 2-D and 3-D environments [42]. This work was further extended later [54], [67]. Since in a medical image, organs may not have sufficiently distinct regional properties, hard constrain that identify object and background seeds is quite necessary to further constraint the search region. Note that users can input seeds interactively. According to desired segmentation results, new seeds can be added to correct segmentation imperfections. Boykov's algorithm can be simply summarized into four steps.

   1) Create an edge-weighted graph according to the image size and dimension.
   2) Input initial object and background seeds.
   3) Associate appropriate edge cost.
   4) Use graph optimization algorithm to solve the minimum *s/t* cut problem.

According to different application, there are two key issues in GCs. One is how to define the hard constrain to initial the segmentation and another is how to design the energy function for minimization. Several other GCs-based research works to segment single object in a medical image have been published later [69]–[76]. The main difference is that they use different hard constrain and energy function for their own applications. For example, Chen *et al.* [70] presented a semisupervised approach for liver computed tomography (CT) segmentation based on GCs framework. In their work, the hard constraints were obtained according to the knowledge of liver characteristic appearance and anatomical location. The energy function considered both knowledge-based similarity measurement and a path-based spatial connectivity measurement. Their model was evaluated on MICCAI2007 liver segmentation challenge datasets and some other data from the hospital. Ye *et al.* [77] proposed an automatic GC segmentation method for lesions in CT using a mean shift super-pixel. They used a 5-D joint spatial, intensity, and shape mean shift clustering to produce super-pixels comprised of intensity and shape index mode maps. The initial object and background seeds were automatically obtained based on shape index concentrations. And their novel energy formulation considered both intensity and shape information. Wolz *et al.* [75] extended Boykov's algorithm to the simultaneous segmentation of a series of magnetic resonance (MR) image acquired from the same subject by extending the graph defined by the energy function from 3-D to 4-D. Shimizu *et al.* [76] proposed two new submodular energies, including shape constrained energy and neighboring structure constrained energy for GCs. Kolmogorov *et al.* [68] studied what energy functions can be minimized via GCs. Grady *et al.* [78] studied the effect of weights a topology on the construction of graphs.

C. Multiobjects Segmentation

Multiobjects segmentation has two situations. The first is to segment multiobjects which belong to the same tissue or organ. For example, the doctor needs to investigate three blood vessels in cardiac MR data. Therefore, we have to segment these blood vessels out. Although it is a multiobject segmentation, if we consider the three blood vessels as the same object, then the virtual problem is still a binary labeling problem which can be solved by above-mentioned single-object segmentation methods. Some example of multiobject segmentation in this case was shown by Boykov *et al.* [42]. The second is to segment multiobjects which belong to different tissues or organs. In this case, the number of labels for assigning to graph nodes is more than two. It is a multilabeling GCs problem virtually. The standard GCs algorithm can find the global optimal solution for binary labeling problem. However, in the multilabeling segmentation case, the minimization of the energy function becomes NP-hard. In order to deal with the multiobjects segmentation problem, Boykov *et al.* [79] proposed the α-expansion-move method and $\alpha\beta$-swap-move method. Although these algorithms cannot find the exact optimal, an approximate optimal solution can be found instead. By using these methods, many multiobjects medical image segmentation problems were solved. Chen *et al.* [46] proposed an automatic anatomy segmentation scheme for body region. The α-expansion-move method was used as the optimization method to delineate the liver, spleen, left kidney, and right kidney simultaneously for abdominal CT dataset. Using this method, calcaneus, tibia, cuboid, talus, and navicular for foot magnetic resonance imaging (MRI) dataset were segmented successfully as well. Figs. 2 and 3 demonstrate the segmentation results by the α-expansion-move method. According to that paper, the delineations within body regions of clinical importance can be accomplished quite rapidly within 1.5 min. The same idea was also used for multiobject recognition of 3-D anatomical structures [80]. Based on the α-expansion-move, Linguraru *et al.* [81] extended basic GCs and proposed a 4-D graph-based method to segment four abdominal organs from multiphase CT data simultaneously. However, the α-expansion method is not practical when the number of objects is too large, leading to an excessive number of expansions that require very high computational complexity. Kofahi *et al.* [82] proposed a novel GCs-based algorithm incorporating the method of α-expansion and graph coloring to solve automatic cell nuclei detection and segmentation problem in histopathology images.
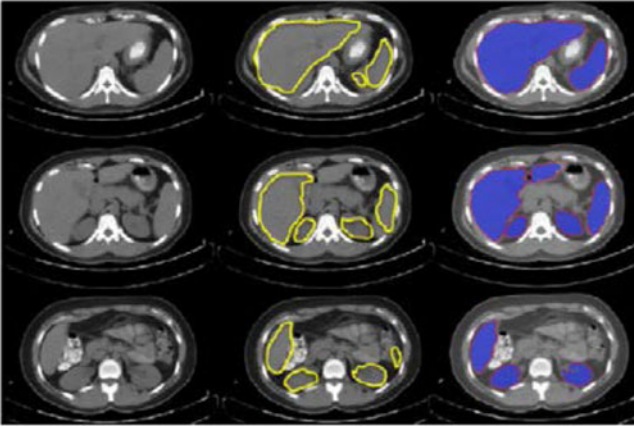
Fig. 2.   Experimental results for multiorgan segmentation are shown in three different anatomical levels for CT abdominal dataset. The first column shows original images slices; the second column indicates the recognized organs; and the third column shows the delineation results yielded by the proposed IGCASM. The contours in the third column show manually delineated organ boundaries. All of the images have been cropped for the best view; original original image size is (512 × 512).
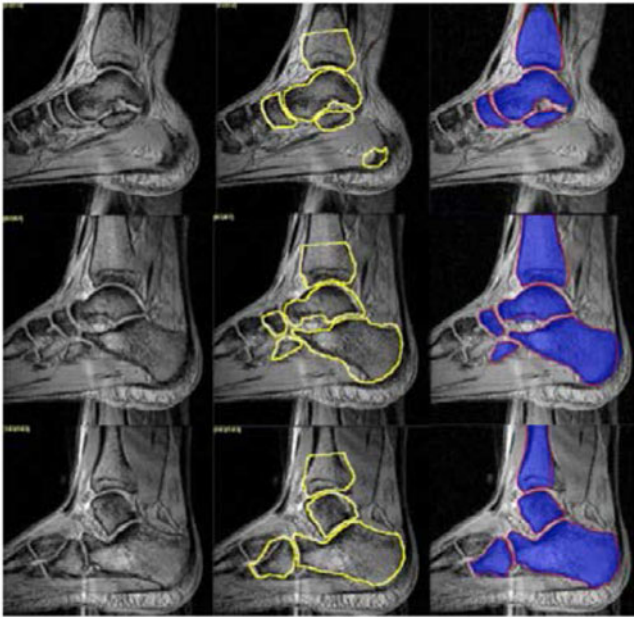

Fig. 3.   Experimental results for multiorgan segmentation are shown in three different anatomical levels for foot MRI dataset. The first column shows original images slices; the second column indicates the recognized organs; and the third column shows the delineation results yielded by the proposed IGCASM. The contours in the third column show manually delineated bone boundaries. All of the images have been cropped for the best view; original original image size is (512 × 512).

D. Multimodality Segmentation

In some practical applications, single-modality medical image cannot provide enough information for radiotherapy treatment planning. For example, the tumor has poor boundary in positron emission tomography (PET) images and low contrast in CT images. Therefore, accurate tumor segmentation in PET
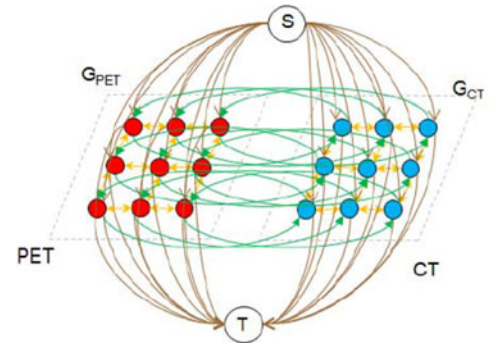

Fig. 4.   Constructed graph with two subgraphs G_{PET} and G_{CT} and d-link arcs encoding the context penalties.

and CT images is challenging. Multimodality imaging technologies are widely used to solve this problem. Take PET-CT as an example, PET-CT effectively integrates the two modalities by making full use of the superior contrast of PET images and superior spatial resolution of CT images. It is possible to acquire both anatomic and functional images of a patient in one single procedure [83]. Although multimodality medical images have been routinely used in clinic, the automatic segmentation tools are still very limited. Most of the existing segmentation algorithms only work for single-modality medical images. Therefore, automatic and accurate segmentation approaches for multimodality medical image are quite necessary. Several research works in this area have been published [84]–[89].

Han *et al.* [86] formulated the joint segmentation problem as an MRF-based segmentation of the image pair with a new energy term that penalized the segmentation difference between PET and CT to achieve tumor segmentation in PET and CT simultaneously. The global optimal solution of the cosegmentation energy function was achieved by computing a single maximum flow. Based on Han's method, Song *et al.* [88] proposed an algorithm for optimal cosegmentation of tumor in PET-CT images by reducing the size of the constructed graph in Han's paper from three subgraphs to two subgraphs. Considered that the tumor volume defined in PET image may not be identical to that defined in CT image, they also employed a soft context cost term to obtain two different segmented tumor contours in PET image and CT image. Motivated by Song's method, a cosegmentation algorithm for lung tumors on PET-CT images based on random walk and GC was recently proposed [89]. In this work, random walk was utilized as an initial preprocessor to provide object seeds for GCs segmentation on PET and CT images. Then, the cosegmentation problem was formulated as an energy minimization problem which can be solved by max-flow/min-cut method. Different from the standard GCs algorithm, a graph including two subgraphs and a special link was constructed as shown in Fig. 4. One subgraph was for the PET image and another was for the CT image. Each subgraph contained *n*-links,

t-links, and the special link *d*-links that encoded a context term, which penalized the difference of the tumor segmentation on the two modalities. To fully utilize the characteristics of PET and CT images, a novel energy representation was devised. PET energy cost, CT energy cost, and the context cost were all included in the energy function by considering downhill feature and 3-D derivate feature. The downhill feature which was intergraded into the PET energy function had great contributions to produce accurate lesion segmentation from PET images and the downhill feature can help to identify the location of the tumor and distinguish the ambiguous area which had similar intensity to the tumor. The 3-D derivate feature enhanced the tumor structures and weakened the background field. Fig. 5 shows some of the segmentation results.

E. GCs With Models

In recent years, there has been an increasing interest in integrating models prior into GCs segmentation framework. GCs approaches have the ability to compute a globally (bilabeling case) or approximate optimal solutions and can enforce piecewise smoothness while preserving relevant sharp discontinuities. However, they are interactive methods. The manual recognition to locate foreground and background object seeds is required through user-interactions. User-input seed points offer good recognition accuracy, especially in 2-D case. However, the segmentation results can be unpredictable along weak edges which always happen in medical images and the user action specifies only roughly the location of the centers of the objects. Neither orientation and scale, nor geographical layout can be exactly defined by user interaction. As an alternative to the manual methods, model-based methods can be employed for initialization/recognition. The advantage of model methods is that even when some object information is missing due to shadowing artifact or speckle, such gaps can be filled by drawing upon the prior information present in the model. Soler *et al.* [90] estimated the position of an organ model by using its histogram. Brejl *et al.* [91] extended the Hough transform to incorporate variability of shape for 2-D segmentations. Although attempting to translate anatomical information into the segmentation framework is promising [25], [90]–[95], these approaches have many drawbacks, such as converging to a local minimum during optimization, large search space, high computational cost, and infeasible platform for multiobject segmentation. The combination of the complementary strengths of GCs and model methods can overcome the weakness of the component methods and achieve a more powerful segmentation tool, where the superior performances and robustness over each of the components are beginning to be well demonstrated.

Vu *et al.* [96] defined a simple fixed shape prior as energy on a shape distance with popular level set approaches. Freedman and Zhang [97] incorporated a shape template into the GCs formulation as a distance function. Malcolm *et al.* [98] imposed a shape model on the terminal edges and performed min-cut iteratively starting with an initial contour. Leventon *et al.* [99] integrated a deformed shape into GCs segmentation, where the shape prior is deformed based on the Gaussian distribution of some
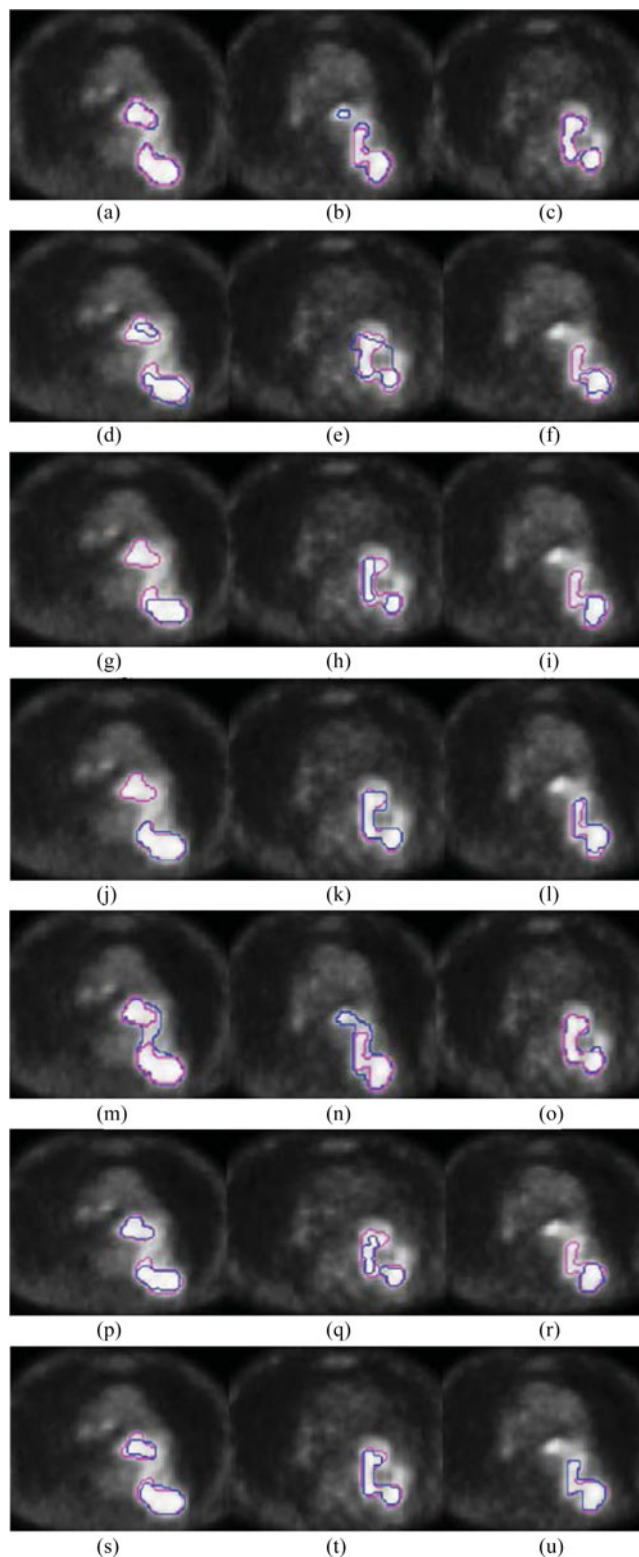

Fig. 5. Three different comparative segmentation results of lesions are shown in each column. The segmentation results on PET (blue) and ground truth (red) are overlaid. (a)–(c) The results by GC conducted solely on PET images. (d)–(f) Segmentation results conducted solely on CT images. (g)–(i) Segmentation results by random walk. (j)–(l) Improved cosegmentation GC method. (m)–(o) Traditional cosegmentation GC method (Song's method [88]). (p)–(r) The results conducted by random walk cosegmentation. (s)–(u) Segmentation results conducted by the method in [89].
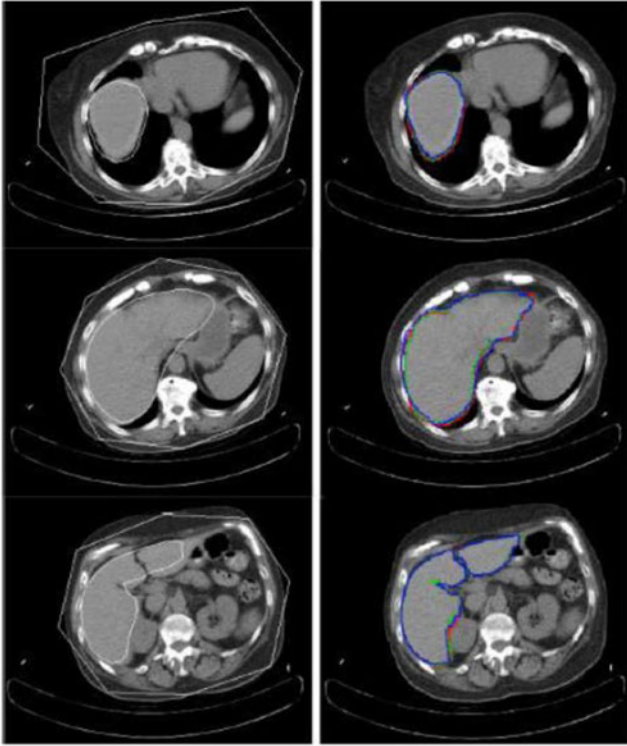
Fig. 6. Experimental results for three slice levels of liver segmentation. The left column is the MOAAM initialization result; the right is the IGC–OAMM result in which the red contour represents reference segmentation: green represents reference segmentation and the blue contour represents segmentation by the proposed method.

predefined geometrical shape statistics. Kohli *et al.* [100] used a simple articulated stickman model together with a conditional random field as the shape prior for performing simultaneous segmentation and 3-D pose estimation of a human body from multiple views. Lempitsky *et al.* [101] used nonparametric kernel densities to model a shape prior and integrated into the GCs. Saito *et al.* [140] optimized the joint segmentation using both of GCs and the shape and location priors.

Integrating the ASM and AAM into GCs also shows advantages. Chen and Bagci [46] proposed a fully automatic 3-D anatomy segmentation method with low computation cost. In this method, an iterative GC active shape model (IGCASM) algorithm was used for object delineation, which effectively combines the rich statistical shape information embodied in ASM with the globally optimal delineation capability of the GC method. The object shape information that generated from the initialization step was integrated into the GCs cost function as a 3-D shape term. This IGCASM method is a 3-D generalization of 2-D GCASM method [102], which is used for 2-D image delineation. This method was tested on a clinical abdominal CT data set with 20 patients and a foot MRI dataset with 11 images. Another novel method combined the AAM, live wire, and GCs for abdominal 3-D organ segmentation [48]. In this method, AAM was used to provide the landmarks to the live wire which in turn improved the shape model of AAM. The segmentation results of liver are illustrated in Fig. 6. The preliminary results of these hybrid methods show that it is feasible to explicitly bring prior 3-D statistical shape information into the GC framework and the hybrid methods show improvement on delineation and can provide practical operational time on clinical images.

III. GRAPH SEARCH

Previously, we have discussed the methods for region segmentation in a medical image. However, sometimes in the medical image, the object required to be segmented is not a region but a 3-D surface. Optimally identifying 3-D object boundaries represented by surfaces is an important task in medical image segmentation and quantitative analysis. The previous discussed GCs method can easily handle the region segmentation problem; however, it is difficult to handle multiple coupled surfaces segmentation. In this section, we introduce another graph theoretic approach, called graph search, to segment surfaces in medical image data. GCs and GS are all cut-based algorithm. The main difference is reflected in how to construct the graph. GS is a sophisticated extension of the *s/t* GC. Both of them need to construct a graph at first and then try to find the minimum cut. However, their way of constructing the graph is different which we will discuss in the following part.

The basic idea of GS is to transform the optimal surface detection problem into seeking a minimum closed set in a node-weighted directed graph. The key to transform the optimal surface detection problem into seeking a minimum closed set in a graph is based on the important observation that any feasible surface in a volumetric image uniquely corresponds to a nonempty closed set in a node-weighted directed graphs with the same cost [103]. And the minimum closed set problem is to search for a closed set with the minimum cost, which can be solved by computing a minimum *s-t* cut. Using this idea, Li *et al.* proposed the 3-D graph-based optimal surface segmentation method which is capable of detecting multiple interacting surfaces simultaneously [104]. This method and its variations were successfully applied to a variety of medical imaging applications, especially retinal layer segmentation of macular optical coherence tomography images [105]–[115]. However, it was limited by the terrain-like shape requirement.

A. Single-Surface Detection

For single-surface detection, the volumetric image is defined as a 3-D matrix $I(x, y, z)$ with image size X, Y, Z. And the surface is defined by a function $S(x, y)$, where $x \in (0,\ldots, X-1)$, $y \in (0, \ldots, Y-1)$, $S(x, y) \in (0, \ldots, Z-1)$. Two smoothness parameters Δx and Δy are designed to guarantee surfaces connectivity in 3-D. More precisely, Δx defines the maximum of $|S(x+1, y) - S(x, y)|$ and Δy defines the maximum of $|S(x, y+1) - S(x, y)|$. A cost function $c(x, y, z)$ which is inversely related to the likelihood that the desired surface contains the voxel is defined. The cost of a surface is the total cost of all voxels on the surface. Therefore, the optimal surface is the one with the minimum cost among all feasible surfaces. A node-weighted directed graph $G(V, E)$ is constructed for the volumetric image. In graph G, every node V corresponds to one and the only one voxel in $I(x, y, z)$ whose cost $w(x, y, z)$ is
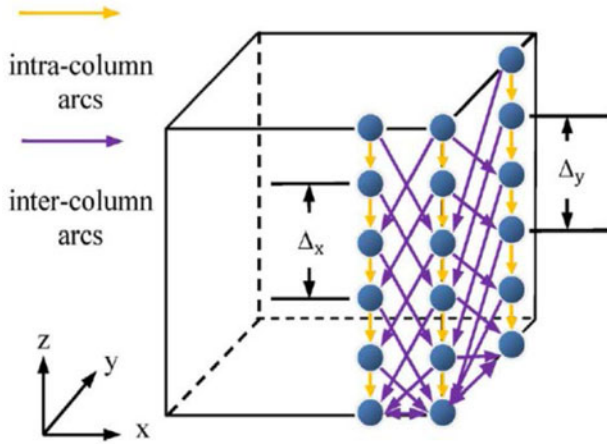
Fig. 7. Illustration of graph construction for single-surface detection.

calculated as follows:

$$w(x,y,z) = \begin{cases} c(x,y,z), & \text{if } z = 0 \\ c(x,y,z) - c(x,y,z-1), & \text{otherwise.} \end{cases}$$

(2)

The arcs of G consist of two types: intracolumn arcs which connect each node with its immediate neighbor below and intercolumn arcs which are constructed according to the smoothness constraints. Fig. 7 shows the construction of a graph. So that the problem of optimal surface detection can be transformed to find a minimum weight closed set by computing a minimum s/t cut [116], [117]. GS for single-surface detection was successfully applied to solve the problem of lung tissue segmentation in CT images of subjects with pathology [115], retinal vessel boundary delineation on fundus images [112], optic disc cup and rim segmentation in 3-D OCT scans [114], retinal layers segmentation in spectral domain optical coherence tomography (SD-OCT) scans of eyes with serous retinal pigment epithelial detachments [110], etc.

B. Multiple Surfaces Detection

For simultaneously segmenting two or more distinct but interrelated surfaces, the optimality is determined by the inherent costs and smoothness properties of individual surfaces as well as surfaces interrelations. Therefore, another set of arcs called intersurface arcs are needed to model the pairwise relations between surfaces. Two parameters $\delta_l \geq 0$ and $\delta_u \geq 0$ are used as a surface separation constraint to represent the minimum distance and the maximum distance between two surfaces separately. The multiple optimal surfaces could be solved simultaneously as a single s/t cut problem by using the maximum-flow algorithm. Li *et al.* [104] applied GS method to ultrasound images and simultaneously segmented lumen-intima and media-adventitia surfaces in intravascular ultrasound datasets. Haeker *et al.* [118] extended this method and used it for macular layer segmentation in 3-D OCT images. Song *et al.* [108] reported a novel algorithm for simultaneous detection of multiple surfaces using both shape and context prior information based on previous GS framework. And their approach showed statistically

significant improvement of segmentation accuracy compared to earlier GS method that was not utilizing shape and context priors. Some of their experiments results are shown in Fig. 8. To segment renal cortex, Li *et al.* [127] extended the multiple surface GS approach. Compared to the traditional multiple surfaces GS approach, it allowed nonuniform sampling distances and physical separation constrains instead of the traditional fixed sampling distance and numerical separation constraints. Their simulation results show that the improved multiple surface GS approach can better separate the renal cortex and renal column.

However, as pointed in [128], these optimal surface detection methods construct the graph and formulate the cost function independently which may lead to ineffective multiple surfaces detection. Therefore, Xiang *et al.* further improved Li's renal cortex segmentation approach [127]. In Xiang's method, a new cost function was formulated based on multiscale boundary detection and a nonuniform graph was constructed. As shown in Fig. 9, each node of a column in G_o for the outer surface or G_i for the inner surface was sampled along the gradient direction in Euclidean distance field of an initial kidney. The sampling steps for each vertex on the outer or inner surface were determined by the distance to the desirable surface. They designed a linear function to map boundary information into a step size, i.e., high boundary information value map to small step size and vice versa. Therefore, sample points are denser in the regional candidate boundaries while they are sparser further from candidate boundaries. Since this approach can control sampling steps, the segmentation accuracy for renal cortex can be improved.

C. Graph Search-Graph Cuts

GS methods can be successfully applied to surface segmentation and GCs methods are widely used for the segmentation of region object. Synergistically combine the GS and GCs methods could be applied to solve more complex and challenging medical image segmentation problems. Dolejší *et al.* [119] showed a semiautomated method to segment the 3-D fluid-associated abnormalities in the retina, so-called symptomatic exudate-associated derangement (SEAD), from 3-D spectral OCT retinal images of subjects suffering from exudative age-related macular degeneration (AMD). AMD is the primary cause of blindness and vision loss among adults [120]. SEAD including intraretinal fluid, subretinal fluid, and pigment epithelial detachment is the main manifestations of AMD. The treatment of AMD is primarily guided by the amount of fluid. Therefore, automated fluid segmentation is quiet necessary. This method had two steps. In the first step, retinal layers were segmented by the optimal surface algorithm [105], [106]. In the second step, the identified layers were used to constrain the segmentation of fluid filled retinal regions using GCs [67]. However, this method required manual interaction and mis-segmentation of layers in the first step which reduced the accuracy of SEAD segmentation. Chen *et al.* [121] further improved it and reported a fully 3-D automated method which effectively combined GS and GCs methods for segmenting the SEADs and layers simultaneously. In Chen's
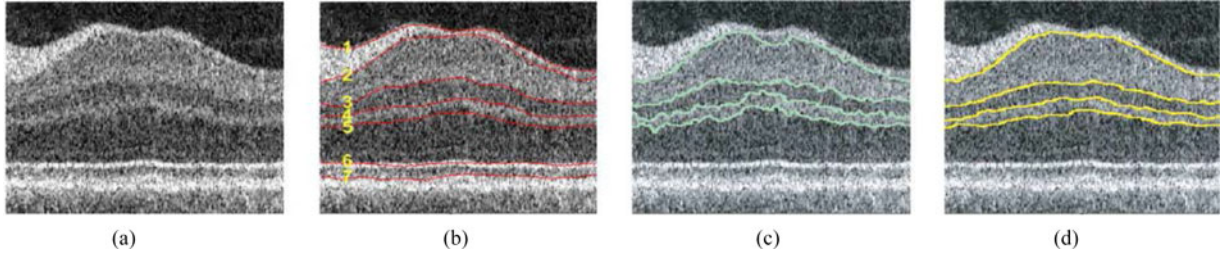
Fig. 8. Intraretinal layer segmentation in 3-D OCT images. (a) A 2-D slice from 3-D retinal OCT dataset. (b) Seven manually labeled surfaces (1–7). (c) Segmentation achieved using the former graph searching approach with only hard constraints—surfaces 2, 3, 4, 5. (d) Segmentation achieved using the proposed algorithm with shape and context prior penalties. (From Song [108].)
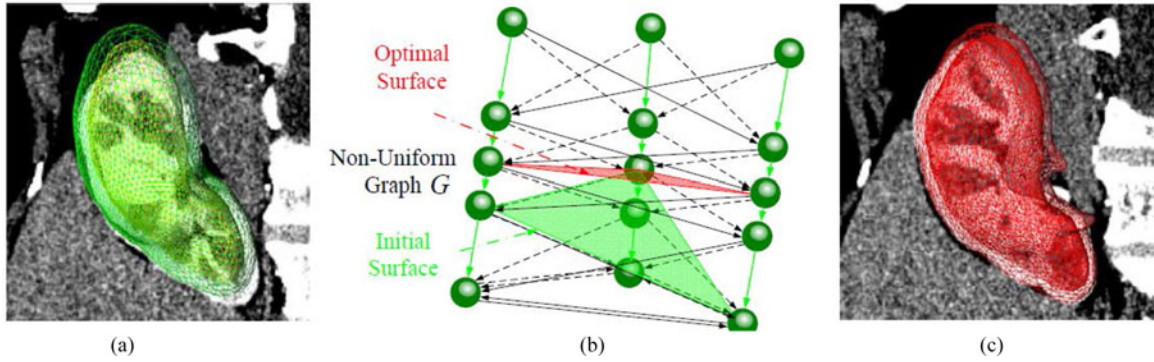

Fig. 9. Nonuniform graph construction. (a) The initialized outer and inner surfaces. (b) The proposed nonuniform graph for optimal surface detection. (c) The refined outer and inner surfaces by using Xiang's nonuniform graph for optimal surface detection.
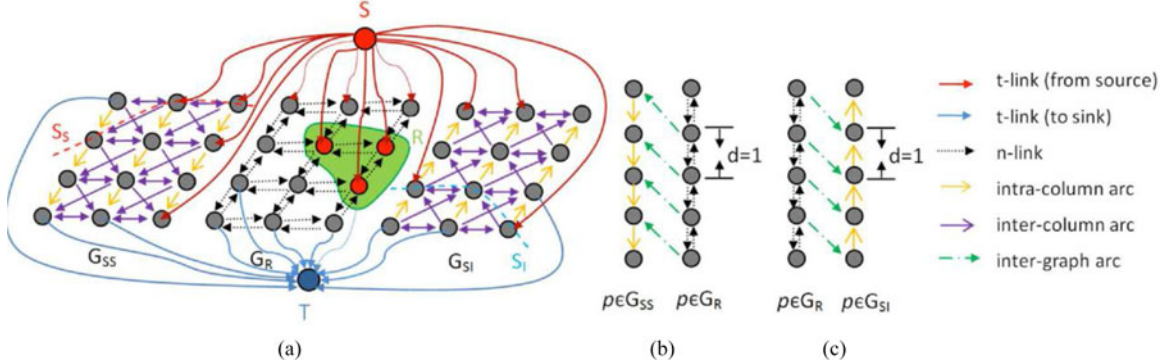

Fig. 10. Illustration of graph construction on a 2-D example. (a) Final constructed graph G which consists of three subgraphs G_{SS}, G_R, and G_{SI}. Note only a part of arcs is shown here. Each node in G_{SS} and G_{SI} is connected to either the source S if the weight <0 or the sink T if the weight >0; and each node in G_R is connected to both S and T. (b) Geometric constraints between surfaces G_{SS} and G_R. (c) Geometric constraints between surfaces G_R and G_{SI}.

method, an automatic voxel classification based on the texture features was used for initialization following the success of their previous works [122], [123]. Probability constraints from the initialization were effectively integrated into the later GS-GCs method to further improve the graph-based segmentation accuracy. The cost function was designed as follows:

$$E(f) = E(\text{Surfaces}) + E(\text{Regions}) + E(\text{Interactions}) \quad (3)$$

where E(Surfaces) represents the cost associated with the segmentation of all surfaces, E(Regions) represents the cost associated with the segmented regions, and E(Interactions) represents the cost of constraints between the surfaces and regions. Probability constraints from the initialization were integrated into the

region term. Superior surface SS and inferior surface SI were included in the interaction term to constrain the region R. For the surfaces SS and SI, subgraphs G_{SS} and G_{SI} were constructed by the GS method [103], respectively. For the region term, the third subgraph G_R was constructed following the GC method [67]. Probability constraints from the initialization were used to define the source and sink seeds for the graphs. These three subgraphs are merged together to form a single s/t graph G which can be solved by a min-cut/max-flow technique [67]. Fig. 10 shows the graph construction. The simulation results showed that compared with the traditional GCs and GS method, the proposed probability constrained GS-GCs method achieved better performance.
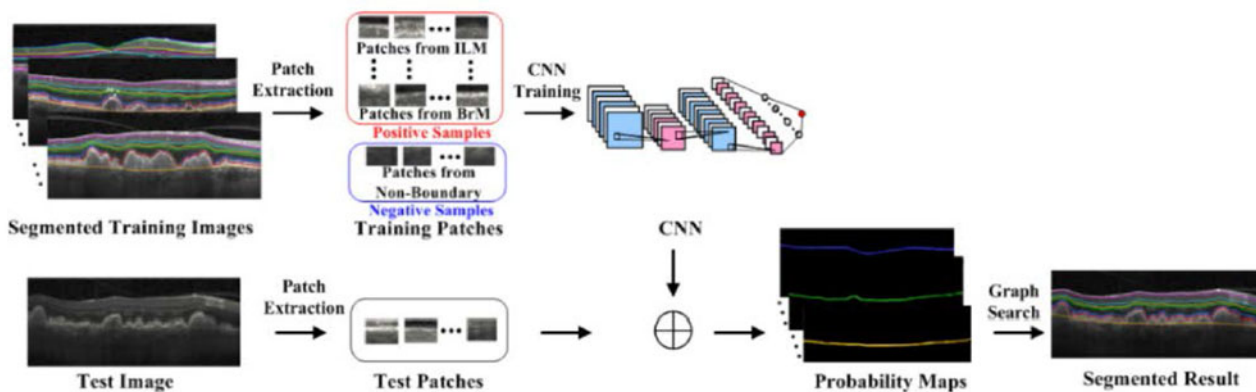
Fig. 11. Outline of the CNN-GS algorithm. (From Fang *et al.* [133].)

IV. CONCLUSION AND DISCUSSION

A. Conclusion

Accurate, robust, and automatic medical image segmentation is an essential component for computer-assisted diagnosis and treatment. Although much work has been done in this research area, medical image segmentation is still a challenging task due to the complex structure of anatomical objects, boundary characteristics of the adjacent organs, and image artifacts and noise resulting from the image acquisition process. GCs and GS techniques are two graph-based segmentation approaches which are successfully applied for 3-D medical image segmentation. This paper systematically reviewed representative GCs/GS-based methods for medical image segmentation. These GCs/ GS-based methods solved the region and surface segmentation problems in medical image processing and can be applied to guide computer-assisted diagnosis and treatment and quantitatively monitor disease progression.

GCs technique has become very popular for region segmentation for medical image due to its ability to compute a globally (bilabeling case) or approximate optimal solutions and can enforce piecewise smoothness while preserving relevant sharp discontinuities. It use hard constrains from the "object" and "background" seeds and additional soft constraints from boundary information, region information or shape information, etc.

GS technique is another graph-theoretic-based approach that has been successfully applied to solve surfaces segmentation problem in medical image field. It converts the surface segmentation problem into seeking a minimum closed set in a node-weighted directed graph and solves the minimum closed set by computing a minimum *s-t* cut.

B. Discussion

Although GCs/ GS methods and their variants have been receiving big success in medical image segmentation, there are still some limitations for the clinic applications. A common problem of graph-based approaches is the computation complexity. Since graph-based approaches use graph as a representation of an image, with the incensement of resolutions, dimensions, and modalities of medical images, the corresponding nodes and edges are dramatically increased. Although parallelizing computation can release the computation burden in some extent [124]–[126], it will still be a problem in the future and limit its clinical applications. Graph-based segmentation approaches convert the medical image segmentation problem into an optimization problem. However, most of the optimization problems are NP-hard to solve. Even researchers try to find an approximate optimal solutions, some of them may result undesirable performance [68]. Another problem for GCs is the "small cut" or shrinking behavior and leakages, which tends to have small segmentations due to minimizing the sum of edge weights in the cut [139].

In past decades, the research of GCs/ GS-based medical image segmentation had been making progress and has been used to solve many practical problems in medical image segmentation. In recent years, the emergence of new algorithms, such as multimodality image technologies, hybrid method, deep learning, etc., provide wider research spaces for them and made the use of GCs/ GS more flexible and more powerful. Noteworthy is the deep learning approaches which achieve strong success recently [129]. Many deep neural network models have been adopted successfully in various fields. Recent works also extended deep learning technique to solve the complex medical image segmentation problem, for example, brain tumor segmentation problem [130], retinal blood segmentation problem [131], pathologic OCT image classification problem [132], etc. Among them, the combination of the deep learning and the traditional method is a new powerful technique which achieved high performance in some aspects [133]–[136]. In recent published work, Fang *et al.* [133] presented a novel framework, called CNN-GS, integrating convolutional neural networks (CNN) with GS method to segment nine-layer boundaries on retinal optical coherence tomography images. Fig. 11 illustrates the outline of the CNN-GS algorithm. CNN-GS method was composed of two main steps. One is CNN layer boundary classification and another is GS layer segmentation based on the CNN probability maps. CNN was used to extract features of retinal layer boundaries and train a classifier. Then, GS method used the probability maps created by the CNN to detect the layer boundary position. Sui *et al.* [134] proposed a similar method for the choroid segmentation of OCT retinal images using

multiscale CNNs combined with GS. Lu *et al.* [135] developed a deep learning algorithm with GC refinement to segment the liver in CT scans. 3-D convolutional neural network was applied to obtain an initial segmentation and learn probability map. GC was then used to refine the initial segmentation. Mukherjee *et al.* [136] proposed a framework for lung nodule segmentation in CT scans using GC with deep learned prior. Their methods embody the robustness of deep learning while retaining the advantage of the traditional-graph-based approaches. Experiment results show that deep-learning-based methods can detect graph structural characteristics and give promising results for graph applications.

GCs and GS techniques are still promising methods for medical image segmentation. Further research could be focused on, first, cosegmentation techniques for multimodality medical images; second, hybrid methods that combine the advanced techniques, such as CNN/deep learning technique, deformable model technique, etc., with GCs/GS to overcome the weakness of each component methods and achieve a more powerful segmentation approach.

References

[1] A. J. Worth, N. Makris, V. S. Caviness, Jr., and D. N. Kennedy, "Neuroanatomical Segmentation in MRI: Technological objectives," *Int. J. Pattern Recognit. Artif. Intell.*, vol. 11, pp. 1161–1187, 1997.

[2] L. P. Clarke *et al.*, "MRI segmentation: Methods and applications," *Magn. Resonance Imag.*, vol. 13, pp. 343–368, 1995.

[3] P. Taylor, "Invited review: Computer aids for decision-making in diagnostic radiology–A literature review," *Brit. J. Radiol.*, vol. 68, pp. 945–957, 1995.

[4] W. E. L. Grimson, G. J. Ettinger, T. Kapur, M. E. Leventon, W. M. Wells, III, and R. Kikinis, "Utilizing segmented MRI data in image-guided surgery," *Int. J. Pattern Recognit. Artif. Intell.*, vol. 11, pp. 1367–1397, 1997.

[5] B. Song and A. Sacan, "Automated wound identification system based on image segmentation and artificial neural networks," in *Proc. IEEE Int. Conf. Bioinformat. Biomed.*, 2012, pp. 1–4.

[6] W. Jentzen, L. Freudenberg, E. G. Eising, M. Heinze, W. Brandau, and A. Bockisch, "Segmentation of PET volumes by iterative image thresholding," *J. Nucl. Med.*, vol. 48, pp. 108–114, 2007.

[7] A. Mustaqeem, A. Javed, and T. Fatima, "An efficient brain tumor detection algorithm using watershed & thresholding based segmentation," *Int. J. Image Graph. Signal Process.*, vol. 4, pp. 34–39, 2012.

[8] R. Wiemker and A. Zwartkruis, "Optimal thresholding for 3D segmentation of pulmonary nodules in high resolution CT," *Int. Congr.*, vol. 1230, pp. 653–658, 2001.

[9] H. Suzuki and J. Toriwaki, "Automatic segmentation of head MRI images by knowledge guided thresholding," *Comput. Med. Imag. Graph., Official J. Comput. Med. Imag. Soc.*, vol. 15, pp. 233–240, 1991.

[10] L. Drever, W. Roa, A. Mcewan, and D. Robinson, "Iterative threshold segmentation for PET target volume delineation," *Med. Phys.*, vol. 34, pp. 1253–1265, 2007.

[11] D. Y. Kim, S. M. Chung, and J. W. Park, "Automatic navigation path generation based on two-phase adaptive region-growing algorithm for virtual angioscopy," *Med. Eng. Phys.*, vol. 28, pp. 339–347, 2006.

[12] T. Xi, R. Schreurs, W. J. Heerink, S. J. Bergé, and T. J. Maal, "A novel region-growing based semi-automatic segmentation protocol for three-dimensional condylar reconstruction using cone beam computed tomography (CBCT)," *PLOS One*, vol. 9, 2014, Art. no. e111126.

[13] K. V. Asari, "A fast and accurate segmentation technique for the extraction of gastrointestinal lumen from endoscopic images," *Med. Eng. Phys.*, vol. 22, pp. 89–96, 2000.

[14] L. Wang, X. Gao, and G. Zhang, "3D region growing algorithm driven by morphological dilation for airway tree segmentation in image guided therapy," *J. Biomed. Eng.*, vol. 30, pp. 679–683, 691, 2013.

[15] J. Rogowska and M. E. Brezinski, "Image processing techniques for noise removal, enhancement and segmentation of cartilage OCT images," *Phys. Med. Biol.*, vol. 47, pp. 641–655, 2002.

[16] Z. Yuqian, G. Weihua, C. Zhencheng, T. Jingtian, and L. Lingyun, "Medical images edge detection based on mathematical morphology," in *Proc. Int. Conf. Eng. Med. Biol. Soc.*, 2005, pp. 6492–6495.

[17] H. R. Singleton and G. M. Pohost, "Automatic cardiac MR image segmentation using edge detection by tissue classification in pixel neighborhoods," Opt. Commun. Center, College Telecommun. Eng., Beijing Univ. Posts Telecommun., Beijing, China, 1999.

[18] A. F. Frangi, D. Rueckert, J. A. Schnabel, and W. J. Niessen, "Automatic construction of multiple-object three-dimensional statistical shape models: Application to cardiac modeling," *IEEE Trans. Med. Imag.*, vol. 21, no. 9, pp. 1151–1166, Sep. 2002.

[19] S. Seifert, A. Barbu, J. Feulner, and M. Suehling, "Hierarchical parsing and semantic navigation of full body CT data," in *Proc. SPIE -Int. Soc. Opt. Eng.*, 2009, vol. 7259, pp. 725902-1–725902-8.

[20] H. Ling, S. K. Zhou, Y. Zheng, B. Georgescu, M. Suehling, and D. Comaniciu, "Hierarchical, learning-based automatic liver segmentation," in *Proc. IEEE Conf. Comput. Vision Pattern Recognit.*, 2008, pp. 1–8.

[21] T. F. Cootes, C. J. Taylor, D. H. Cooper, and J. Graham, "Active shape models-their training and application," *Comput. Vision Image Understanding*, vol. 61, pp. 38–59, 1995.

[22] T. F. Cootes, A. Hill, C. J. Taylor, and J. Haslam, "The use of active shape models for locating structures in medical images," *Image Vision Comput.*, vol. 12, pp. 355–365, 1993.

[23] S. C. Mitchell, B. P. F. Lelieveldt, d. G. Van, Rob J., H. G. Bosch, J. H. C. Reiver, and M. Sonka, "Multistage hybrid active appearance model matching: Segmentation of left and right ventriclesin cardiac MR images," *IEEE Trans. Med. Imag.*, vol. 20, no. 5, pp. 415–423, May 2001.

[24] T. F. Cootes, G. J. Edwards, and C. J. Taylor, "Active appearance models," *IEEE Trans. Pattern Anal. Mach. Intell.*, vol. 23, no. 6, pp. 681–685, Jun. 2001.

[25] S. C. Mitchell, J. G. Bosch, B. P. F. Lelieveldt, R. J. van der Geest, J. H. C. Reiber, and M. Sonka, "3-D active appearance models: Segmentation of cardiac MR and ultrasound images," *IEEE Trans. Med. Imag.*, vol. 21, no. 9, pp. 1167–1178, Sep. 2002.

[26] R. Beichel, H. Bischof, F. Leberl, and M. Sonka, "Robust active appearance models and their application to medical image analysis," *IEEE Trans. Med. Imag.*, vol. 24, no. 9, pp. 1151–1169, Sep. 2005.

[27] J. Hansegard, S. Urheim, K. Lunde, and S. I. Rabben, "Constrained active appearance models for segmentation of triplane echocardiograms," *IEEE Trans. Med. Imag.*, vol. 26, no. 10, pp. 1391–400, Oct. 2007.

[28] J. A. Sethian, *Level Set Methods and Fast Marching Methods*, 2nd ed. Cambridge, U.K.: Cambridge Univ. Press, 1999.

[29] S. Osher and R. Fedkiw, *Level Set Methods and Dynamic Implicit Surfaces*. New York, NY, USA: Springer, 2003.

[30] Y. Jing and J. S. Duncan, "3D image segmentation of deformable objects with joint shape-intensity prior models using level sets," *Med. Image Anal.*, vol. 8, pp. 285–294, 2004.

[31] R. Malladi, J. A. Sethian, and B. C. Vemuri, "Shape modeling with front propagation: A level set approach," *IEEE Trans. Pattern Anal. Mach. Intell.*, vol. 17, no. 2, pp. 158–175, Feb. 1995.

[32] D. Cremers, S. J. Osher, and S. Soatto, "Kernel density estimation and intrinsic alignment for shape priors in level set segmentation," *Int. J. Comput. Vision*, vol. 69, pp. 335–351, 2006.

[33] C. T. Zahn, "Graph-theoretical methods for detecting and describing gestalt clusters," *IEEE Trans. Comput.*, vol. C-20, no. 1, pp. 68–86, Jan. 1971.

[34] S. H. Kwok and A. G. Constantinides, "A fast recursive shortest spanning tree for image segmentation and edge detection," *IEEE Trans. Image Process.*, vol. 6, no. 2, pp. 328–332, Feb. 1997.

[35] P. F. Felzenszwalb and D. P. Huttenlocher, "Efficient graph-based image segmentation," *Int. J. Comput. Vision*, vol. 59, pp. 167–181, 2004.

[36] Y. Xu and E. C. Uberbacher, "2D image segmentation using minimum spanning trees," *Image Vision Comput.*, vol. 15, pp. 47–57, 1997.

[37] A. X. Falcão and J. K. Udupa, "A 3D generalization of user-steered live-wire segmentation," *Med. Image Anal.*, vol. 4, pp. 389–402, 2000.

[38] A. X. Falcão, J. Stolfi, and A. L. R. De, "The image foresting transform: Theory, algorithms, and applications," *IEEE Trans. Pattern Anal. Mach. Intell.*, vol. 26, no. 1, pp. 19–29, Jan. 2004.

[39] R. Ardon and L. D. Cohen, "Fast constrained surface extraction by minimal paths," *Int. J. Comput. Vision*, vol. 69, pp. 127–136, 2006.

[40] L. Grady, "Minimal surfaces extend shortest path segmentation methods to 3D," *IEEE Trans. Pat. Anal. Mach. Intell.*, vol. 32, pp. 321–334, 2010.

[41] M. Sonka, M. D. Winniford, and S. M. Collins, "Robust simultaneous detection of coronary borders in complex images," *IEEE Trans. Med. Imag.*, vol. 14, no. 1, pp. 151–161, Mar. 1995.

[42] Y. Boykov and M. P. Jolly, "Interactive organ segmentation using graph cuts," in *Proc. Int. Conf. Med. Image Comput. Comput.-Assisted Intervention* (Lecture Notes Comput. Sci., vol. 1935), 2000, pp. 276–286.

[43] Y. Y. Boykov and M. P. Jolly, "Interactive graph cuts for optimal boundary & region segmentation of objects in N-D images," in *Proc. Int. Conf. Comput. Vision*, 2001, pp. 105–112.

[44] Y. Y. Boykov, O. Veksler, and R. Zabih, "Efficient approximate energy minimization via graph cuts," *IEEE Trans. Pattern Anal. Mach. Intell.*, vol. 20, no. 12, pp. 1222–1239, Nov. 2001.

[45] W. Ju, D. Xiang, B. Zhang, L. Wang, I. Kopriva, and X. Chen, "Random walk and graph cut for co-segmentation of lung tumor on PET-CT images," *IEEE Trans. Image Process.*, vol. 24, no. 12, pp. 5854–5867, Dec. 2015.

[46] X. Chen and U. Bagci, "3D automatic anatomy segmentation based on iterative graph-cut-ASM," *Med. Phys.*, vol. 38, pp. 4610–4622, 2011.

[47] X. Chen, M. Niemeijer, L. Zhang, K. Lee, D. A. Michael, and M. Sonka, "3D segmentation of fluid-associated abnormalities in retinal OCT: Probability constrained graph-search–graph-cut," *IEEE Trans. Med. Imag.*, vol. 31, no. 8, pp. 1521–1531, Aug. 2012.

[48] X. Chen, J. K. Udupa, U. Bagci, Y. Zhuge, and J. Yao, "Medical image segmentation by combining graph cut and oriented active appearance models," *IEEE Trans. Image Process.*, vol. 21, no. 4, pp. 2035–2046, Apr. 2012.

[49] G. G. Slabaugh, G. Unal, T. Fang, and H. N. Doan, "System and method for segmentation of anatomical structures in MRI volumes using graph cuts," U.S. Patent 8379957 B2, Feb. 2013.

[50] R. Beichel *et al.*, "Liver segmentation in contrast enhanced CT data using graph cuts and interactive 3D segmentation refinement methods," *Med. Phys.*, vol. 39, pp. 1361–1373, 2012.

[51] S. Esneault, C. Lafon, and J. L. Dillenseger, "Liver vessels segmentation using a hybrid geometrical moments/graph cuts method," *IEEE Trans. Biomed. Eng.*, vol. 57, no. 2, pp. 276–283, Feb. 2010.

[52] H. Shim, S. Chang, C. Tao, J. H. Wang, D. Kaya, and K. T. Bae, "Semi-automated segmentation of kidney from high-resolution multidetector computed tomography images using a graph-cuts technique," *J. Comput. Assisted Tomography*, vol. 33, pp. 893–901, 2009.

[53] D. Mahapatra and J. M. Buhmann, "Prostate MRI segmentation using learned semantic knowledge and graph cuts," *IEEE Trans. Biomed. Eng.*, vol. 61, no. 3, pp. 756–764, Mar. 2014.

[54] Y. Boykov and V. Kolmogorov, "An experimental comparison of min-cut/max-flow algorithms for energy minimization in vision," *IEEE Trans. Pattern Anal. Mach. Intell.*, vol. 26, no. 9, pp. 1124–1137, Sep. 2004.

[55] D. L. Pham, C. Xu, and J. L. Prince, "A survey of current methods in medical image segmentation," *Annu. Rev. Biomed. Eng.*, vol. 2, pp. 315–337, 2000.

[56] D. L. Pham, C. Xu, and J. L. Prince, "Current methods in medical image segmentation," *Biomed. Eng.*, vol. 2, pp. 315–337, 2000.

[57] J. A. Noble and D. Boukerroui, "Ultrasound image segmentation: A survey," *IEEE Trans. Med. Imag.*, vol. 25, no. 8, pp. 987–1010, Aug. 2006.

[58] A. W. Liew, "Current methods in the automatic tissue segmentation of 3D magnetic resonance brain images," *Curr. Med. Imag. Rev.*, vol. 2, pp. 91–103(13), 2006.

[59] S. Masood, M. Sharif, A. Masood, M. Yasmin, and M. Raza, "A survey on medical image segmentation," *Curr. Med. Imag. Rev.*, vol. 11, pp. 3–14, 2015.

[60] N. Sharma and L. M. Aggarwal, "Automated medical image segmentation techniques," *J. Med. Phys.*, vol. 35, pp. 3–14, 2010.

[61] S. Geman and C. Graffigne, "Markov random field image models and their applications to computer vision," in *Proc. Int. Congr. Math*, 1986, pp. 1496–1517.

[62] A. V. Goldberg and R. E. Tarjan, "A new approach to the maximum-flow problem," *J. ACM*, vol. 35, pp. 921–940, 1988.

[63] E. Jack and M. K. Richard, *Theoretical Improvements in Algorithmic Efficiency for Network Flow Problems*. New York, NY, USA: Springer, 1972.

[64] A. V. Goldberg and S. Rao, "Beyond the flow decomposition barrier," *J. ACM*, vol. 45, pp. 783–797, 1997.

[65] B. V. Cherkassky and A. V. Goldberg, "On implementing the push—relabel method for the maximum flow problem," *Algorithmica*, vol. 19, pp. 390–410, 1997.

[66] D. R. Fulkerson, "Flows in networks," *Recent Adv. Math. Program.*, vol. 18, pp. 319–331, 1962.

[67] Y. Boykov and G. Funkalea, "Graph cuts and efficient N-D image segmentation," *Int. J. Comput. Vision*, vol. 70, pp. 109–131, 2006.

[68] V. Kolmogorov and R. Zabih, "What energy functions can be minimized via graph cuts?" *IEEE Trans. Pattern Anal. Mach. Intell.*, vol. 26, no. 2, pp. 147–159, Feb. 2002.

[69] A. I. Ben, K. Punithakumar, S. Li, A. Islam, and J. Chong, *Left Ventricle Segmentation via Graph Cut Distribution Matching*. Berlin, Germany: Springer, 2009.

[70] Y. Chen, Z. Wang, J. Hu, W. Zhao, and Q. Wu, "The domain knowledge based graph-cut model for liver CT segmentation," *Biomed. Signal Process. Control*, vol. 7, pp. 591–598, 2012.

[71] R. Juang, E. R. Mcveigh, B. Hoffmann, D. Yuh, and P. Burlina, "Automatic segmentation of the left-ventricular cavity and atrium in 3D ultrasound using graph cuts and the radial symmetry transform," *Proc. IEEE Int. Symp. Biomed. Imag., From Nano To Macro*, 2011, vol. 7906, pp. 606–609.

[72] S. A. Sadananthan, W. Zheng, M. W. L. Chee, and V. Zagorodnov, "Skull stripping using graph cuts," *Neuroimage*, vol. 49, pp. 225–239, 2009.

[73] L. Liang, K. Rehm, R. P. Woods, and D. A. Rottenberg, "Automatic segmentation of left and right cerebral hemispheres from MRI brain volumes using the graph cuts algorithm," *Neuroimage*, vol. 34, pp. 1160–1170, 2007.

[74] F. V. D. Lijn, T. D. Heijer, M. M. B. Breteler, and W. J. Niessen, "Hippocampus segmentation in MR images using atlas registration, voxel classification, and graph cuts," *Neuroimage*, vol. 43, pp. 708–720, 2008.

[75] R. Wolz *et al.*, "Measurement of hippocampal atrophy using 4D graph-cut segmentation: Application to ADNI," *Neuroimage*, vol. 52, pp. 109–118, 2010.

[76] A. Shimizu *et al.*, *Automated Segmentation of 3D CT Images Based on Statistical Atlas and Graph Cuts*. Berlin, Germany: Springer, 2010.

[77] X. Ye, G. Beddoe, and G. Slabaugh, "Automatic graph cut segmentation of lesions in CT using mean shift superpixels," *Int. J. Biomed. Imag.*, vol. 2010, 2010, Art. no. 983963.

[78] L. Grady and M. P. Jolly, "Weights and topology: A study of the effects of graph construction on 3D image segmentation," in *Proc. Int. Conf. Med. Image Comput. Comput.-Assisted Intervention*, 2010, pp. 153–161.

[79] Y. Boykov, O. Veksler, and R. Zabih, "Fast approximate energy minimization via graph cuts," *IEEE Trans. Pattern Anal. Mach. Intell.*, vol. 23, no. 11, pp. 1222–1239, Nov. 2001.

[80] U. Bagci, X. Chen, and J. K. Udupa, "Hierarchical scale-based multiobject recognition of 3-D anatomical structures," *IEEE Trans. Med. Imag.*, vol. 31, no. 3, pp. 777–789, Mar. 2012.

[81] M. G. Linguraru, J. A. Pura, V. Pamulapati, and R. M. Summers, "Statistical 4D graphs for multi-organ abdominal segmentation from multiphase CT," *Med. Image Anal.*, vol. 16, pp. 904–914, 2012.

[82] Y. Al-Kofahi, W. Lassoued, W. Lee, and B. Roysam, "Improved automatic detection and segmentation of cell nuclei in histopathology images," *IEEE Trans. Biomed. Eng.*, vol. 57, no. 4, pp. 841–852, Apr. 2010.

[83] C. Greco, K. Rosenzweig, G. L. Cascini, and O. Tamburrini, "Current status of PET/CT for tumour volume definition in radiotherapy treatment planning for non-small cell lung cancer (NSCLC)," *Lung Cancer*, vol. 57, pp. 125–134, 2007.

[84] U. Bagci *et al.*, "Joint segmentation of anatomical and functional images: Applications in quantification of lesions from PET, PET-CT, MRI-PET, and MRI-PET-CT images," *Med. Image Anal.*, vol. 17, pp. 929–945, 2013.

[85] U. Bagci, J. K. Udupa, J. Yao, and D. J. Mollura, "Co-segmentation of functional and anatomical images," in *Proc. Int. Conf. Med. Image Comput. Comput.-Assisted Intervention*, 2012, pp. 459–467.

[86] D. Han *et al.*, "Globally optimal tumor segmentation in PET-CT images: A graph-based co-segmentation method," in *Proc. Int. Conf. Inf. Process. Med. Imag.*, 2011, pp. 245–256.

[87] X. Wang, C. Ballangan, H. Cui, and M. Fulham, "Lung tumor delineation based on novel tumor-background likelihood models in PET-CT images," *IEEE Trans. Nucl. Sci.*, vol. 61, no. 1, pp. 218–224, Feb. 2014.

[88] Q. Song *et al.*, "Optimal co-segmentation of tumor in PET-CT images with context information," *IEEE Trans. Med. Imag.*, vol. 32, no. 9, pp. 1685–1697, Sep. 2013.

[89] W. Ju, D. Xiang, B. Zhang, and L. Wang, "Random walk and graph cut for co-segmentation of lung tumor on PET-CT images," *IEEE Trans. Image Process.*, vol. 24, no. 12, pp. 5854–5867, Dec. 2015.

[90] S. Luc *et al.*, "Fully automatic anatomical, pathological, and functional segmentation from CT scans for hepatic surgery," *Comput. Aided Surg.*, vol. 6, pp. 131–142, 2001.

[91] M. Brejl and M. Sonka, "Object localization and border detection criteria design in edge-based image segmentation: Automated learning from examples," *IEEE Trans. Med. Imag.*, vol. 19, no. 10, pp. 973–985, Oct. 2000.

[92] J. G. Bosch *et al.*, "Automatic segmentation of echocardiographic sequences by active appearance motion models," *IEEE Trans. Med. Imag.*, vol. 21, no. 11, pp. 1374–1383, Nov. 2002.

[93] Y. Chen *et al.*, "Using prior shapes in geometric active contours in a variational framework," *Int. J. Comput. Vision*, vol. 50, pp. 315–328, 2002.

[94] L. Gong, S. D. Pathak, D. R. Haynor, P. S. Cho, and Y. Kim, "Parametric shape modeling using deformable superellipses for prostate segmentation," *IEEE Trans. Med. Imag.*, vol. 23, no. 3, pp. 340–349, Mar. 2004.

[95] D. Shen, Y. Zhan, and C. Davatzikos, "Segmentation of prostate boundaries from ultrasound images using statistical shape model," *IEEE Trans. Med. Imag.*, vol. 22, no. 4, pp. 539–551, Apr. 2003.

[96] N. Vu and B. S. Manjunath, "Shape prior segmentation of multiple objects with graph cuts," in *Proc. IEEE Conf. Comput. Vision Pattern Recognit.*, 2008, pp. 1–8.

[97] D. Freedman and T. Zhang, "Interactivegraph cut based segmentation with shape priors," in *Proc. IEEE Comput. Soc. Conf. Comput. Vision Pattern Recognit.*, 2005, vol. 1, pp. 755–762.

[98] J. Malcolm, Y. Rathi, and A. Tannenbaum, "Graph cut segmentation with nonlinear shape priors," in *Proc. Int. Conf. Image Process.*, 2007, pp. IV-365–IV-368.

[99] M. E. Leventon, W. E. L. Grimson, and O. Faugeras, "Statistical shape influence in geodesic active contours," in *Proc. IEEE Conf. Comput. Vision Pattern Recognit.*, 2000, pp. 316–323.

[100] P. Kohli, J. Rihan, M. Bray, and P. H. Torr, "Simultaneous segmentation and pose estimation of humans using dynamic graph cuts," *Int. J. Comput. Vision*, vol. 79, pp. 285–298, 2010.

[101] V. Lempitsky, A. Blake, and C. Rother, "Image segmentation by branch-and-mincut," in *Proc. Comput. Vision, Eur. Conf. Comput. Vision*, Marseille, France, Oct. 12–18, 2008, pp. 15–29.

[102] X. Chen, J. K. Udupa, and U. Bagci, "3D automatic anatomy recognition based on iterative graph-cut-ASM," in *Proc. SPIE Int. Soc. Opt. Eng.*, vol. 7625, pp. 4610–4622, 2010.

[103] X. Wu and D. Z. Chen, "Optimal net surface problems with applications," in *Proc. Int. Colloquium Automata, Lang. Program.*, Malaga, Spain, Jul. 8–13, 2002, pp. 1029–1042

[104] K. Li, X. Wu, D. Z. Chen, and M. Sonka, "Optimal surface segmentation in volumetric images—A graph-theoretic approach," *IEEE Trans. Pattern Anal. Mach. Intell.*, vol. 28, no. 1, pp. 119–134, Jan. 2006.

[105] M. K. Garvin, M. D. Abramoff, R. Kardon, S. R. Russell, X. Wu, and M. Sonka, "Intraretinal layer segmentation of macular optical coherence tomography images using optimal 3-D graph search," *IEEE Trans. Med. Imag.*, vol. 27, no. 10, pp. 1495–1505, Oct. 2008.

[106] M. K. Garvin, M. D. Abràmoff, X. Wu, S. R. Russell, T. L. Burns, and M. Sonka, "Automated 3-D intraretinal layer segmentation of macular spectral-domain optical coherence tomography images," *IEEE Trans. Med. Imag.*, vol. 28, no. 9, pp. 1436–1447, Sep. 2009.

[107] K. M. Lee, "Segmentations of the intraretinal surfaces, optic disc and retinal blood vessels in 3D-OCT scans," Ph.D. dissertation, University of Iowa, Iowa City, IA, USA, 2009.

[108] Q. Song, J. Bai, M. K. Garvin, M. Sonka, J. M. Buatti, and X. Wu, "Optimal multiple surface segmentation with shape and context priors," *IEEE Trans. Med. Imag.*, vol. 32, no. 2, pp. 376–386, Feb. 2013.

[109] P. A. Dufour, L. Ceklic, H. Abdillahi, and S. Schroder, "Graph-based multi-surface segmentation of OCT data using trained hard and soft constraints," *IEEE Trans. Med. Imag.*, vol. 32, no. 3, pp. 531–543, Mar. 2013.

[110] F. Shi *et al.*, "Automated 3-D retinal layer segmentation of macular optical coherence tomography images with serous pigment epithelial detachments," *IEEE Trans. Med. Imag.*, vol. 34, no. 2, pp. 441–452, Feb. 2015.

[111] F. Zhao *et al.*, "Congenital aortic disease: 4D magnetic resonance segmentation and quantitative analysis," *Med. Image Anal.*, vol. 13, pp. 483–493, 2007.

[112] X. Xu *et al.*, "Vessel boundary delineation on fundus images using graph-based approach," *IEEE Trans. Med. Imag.*, vol. 30, no. 6, pp. 1184–1191, Jun. 2011.

[113] X. Chen, M. Niemeijer, L. Zhang, K. Lee, M. D. Abramoff, and M. Sonka, "Three-dimensional segmentation of fluid-associated abnormalities in retinal OCT: Probability constrained graph-search-graph-cut," *IEEE Trans. Med. Imag.*, vol. 31, no. 8, pp. 1521–1531, Aug. 2012.

[114] K. Lee *et al.*, "Segmentation of the optic disc in 3-D OCT scans of the optic nerve head," *IEEE Trans. Med. Imag.*, vol. 29, no. 1, pp. 159–168, Jan. 2010.

[115] P. Hua, Q. Song, M. Sonka, and E. A. Hoffman, "Segmentation of pathological and diseased lung tissue in CT images using a graph-search algorithm," in *Proc. IEEE Int. Symp. Biomed. Imag., From Nano To Macro*, 2011, pp. 2072–2075.

[116] X. Wu and D. Z. Chen, "Optimal net surface problems with applications," in *Proc. Int. Colloquium Automata, Lang., Program. (*Lecture Notes Comput. Sci., vol. 2380), 2002, pp. 1029–1042.

[117] D. S. Hochbaum, "A new-old algorithm for minimum-cut and maximum-flow in closure graphs," *Networks*, vol. 37, pp. 171–193, 2001.

[118] M. Haeker, M. Sonka, V. A. Shah, and X. Wu, "Automated segmentation of intraretinal layers from macular optical coherence tomography images," in *Proc. SPIE-Int. Soc. Opt. Eng.*, vol. 6512, pp. 651214-1–651214-11, 2007.

[119] M. Dolejší, M. D. Abràmoff, M. Sonka, and J. Kybic, "Semi-automated segmentation of symptomatic exudate-associated derangements (SEADs) in 3D OCT using layer segmentation," *Anal. Biomed. Signals Images*, vol. 6159, pp. 27–32, 2010.

[120] N. M. Bressler, "Age-related macular degeneration is the leading cause of blindness," *J. Amer. Med. Assoc.*, vol. 291, pp. 1900–1901, 2004.

[121] X. Chen, M. Niemeijer, L. Zhang, K. Lee, M. D. Abràmoff, and M. Sonka, "3D segmentation of fluid-associated abnormalities in retinal OCT: Probability constrained graph-search–graph-cut," *IEEE Trans. Med. Imag.*, vol. 31, no. 8, pp. 1521–1531, Aug. 2012.

[122] G. Quellec, K. Lee, M. Dolejsi, M. K. Garvin, M. D. Abràmoff, and M. Sonka, "Three-dimensional analysis of retinal layer texture: Identification of fluid-filled regions in SD-OCT of the macula," *IEEE Trans. Med. Imag.*, vol. 29, no. 6, pp. 1321–1330, Jun. 2010.

[123] M. Niemeijer *et al.*, "Automated estimation of fluid volume in 3D OCT scans of patients with CNV due to AMD," *Investigative Ophthalmol. Vis. Sci.*, vol. 53, 2012, Art. no. 4074.

[124] M. Yu, S. Shen, and Z. Hu, "Dynamic parallel and distributed graph cuts," *IEEE Trans. Image Process.*, vol. 25, no. 12, pp. 61–66, Dec. 2015.

[125] P. Strandmark and F. Kahl, "Parallel and distributed graph cuts by dual decomposition," in *Proc. IEEE Conf. Comput. Vision Pattern Recognit.*, 2010, pp. 2085–2092.

[126] J. Liu and J. Sun, "Parallel graph-cuts by adaptive bottom-up merging," in *Proc. IEEE Conf. Comput. Vision Pattern Recognit.*, 2010, pp. 2181–2188.

[127] X. Li, X. Chen, J. Yao, X. Zhang, F. Yang, and J. Tian, "Automatic renal cortex segmentation using implicit shape registration and novel multiple surfaces graph search," *IEEE Trans. Med. Imag.*, vol. 31, no. 10, pp. 1849–1860, Oct. 2012.

[128] D. Xiang *et al.*, "CorteXpert: A model-based method for automatic renal cortex segmentation," *Med. Image Anal.*, vol. 42, pp. 257–273, Oct. 2017.

[129] Y. Lecun, Y. Bengio, and G. Hinton, "Deep learning," *Nature*, vol. 521, pp. 436–444, 2015.

[130] S. Pereira, A. Pinto, V. Alves, and C. A. Silva, "Brain tumor segmentation using convolutional neural networks in MRI images," *IEEE Trans. Med. Imag.*, vol. 35, no. 5, pp. 1240–1251, May 2016.

[131] P. Liskowski and K. Krawiec, "Segmenting retinal blood vessels with deep neural networks," *IEEE Trans. Med. Imag.*, vol. 35, no. 11, pp. 2369–2380, Nov. 2016.

[132] S. P. K. Karri, D. Chakraborty, and J. Chatterjee, "Transfer learning based classification of optical coherence tomography images with diabetic macular edema and dry age-related macular degeneration," *Biomed. Opt. Express*, vol. 8, pp. 579–592, 2017.

[133] L. Fang *et al.*, "Automatic segmentation of nine retinal layer boundaries in OCT images of non-exudative AMD patients using deep learning and graph search," *Biomed. Opt. Express*, vol. 8, pp. 2732–2744, 2017.

[134] X. Sui *et al.*, "Choroid segmentation from optical coherence tomography with graph-edge weights learned from deep convolutional neural networks," *Neurocomputing*, vol. 237, pp. 332–341, 2017.

[135] F. Lu *et al.*, "Automatic 3D liver location and segmentation via convolutional neural network and graph cut," *Int. J. Comput. Assisted Radiol. Surgery*, vol. 12, pp. 171–182, 2017.

[136] S. Mukherjee, X. Huang, and R. R. Bhagalia, "Lung nodule segmentation using deep learned prior based graph cut," in *Proc. IEEE Int. Symp. Biomed. Imag.*, 2017, pp. 1205–1208.

[137] M. Sonka, V. Hlavac, and R. Boyle, *Image Processing, Analysis, and Machine Vision*. Mobile, AL, USA: Thomson, 2007.

[138] O. Lezoray and L. Grady, *Image Processing and Analysis With Graphs: Theory and Practice*. Boca Raton, FL, USA: CRC Press, 2017.

[139] S. Hanaoka *et al.*, "3-D graph cut segmentation with riemannian metrics to avoid the shrinking problem," *MICCAI*, vol. 14, pt. 3, pp. 554–561, 2011.

[140] Saito *et al.*, "Fast approximation for joint optimization of segmentation, shape, and location priors, and its application in gallbladder segmentation," *Int. J. Comput. Assisted Radiol. Surgery*, vol. 12, no. 5, pp. 743–756, 2017.

Xinjian Chen (SM'15) received the Ph.D. degree in pattern recognition and machine intelligence from the Institute of Automation, Chinese Academy of Sciences, Beijing, China, in 2006.

He is a Distinguished Professor with the School of Electrical and Information Engineering, Soochow University, Suzhou, China, and the Director of Medical Image Processing, Analysis and Visualization Laboratory. He has authored or coauthored more than 100 papers in prestigious journals and conferences, including IEEE TRANSACTIONS ON MEDICAL IMAGING, IEEE TRANSACTIONS ON BIOMEDICAL ENGINEERING, etc. His research interests include medical image processing and analysis, pattern recognition, and machine learning.

Dr. Chen has served as Associate Editor for the IEEE TRANSACTIONS ON MEDICAL IMAGING and the IEEE JOURNAL OF TRANSLATIONAL ENGINEERING IN HEALTH AND MEDICINE.

Lingjiao Pan received the M.D. degree from the Gwangju Institute of Science and Technology, Gwangju, South Korea, in 2007. She is currently working toward the Ph.D. degree in medical imaging at the School of Electrical and Information Engineering, Soochow University, Suzhou, China.

She worked as an R&D Engineer with LG Electronics (2007–2008) and with Electronics and Telecommunications Research Institute (2008–2011), South Korea. Since 2012, she has been working as an Assistant Professor with the School of Electrical and Information Engineering, Jiangsu University of Technology, Jiangsu, China. Her research interests include medical image processing and analysis and data compression.